

Article

Analysis of Reservoir Fluid Migration in the Process of CO₂ Sequestration in a Partially Depleted Gas Reservoir

Wiesław Szott *  and Krzysztof Miłek 

Department of Hydrocarbon Reservoir and UGS Simulation, Oil and Gas Institute—National Research Institute, Lubicz 25A, 31-504 Krakow, Poland; milek@inig.pl

* Correspondence: szott@inig.pl; Tel.: +48-134-368-941

Abstract: This paper addresses problems of reservoir fluid migrations in the process of CO₂ sequestration in a partially depleted petroleum reservoir. A detailed analysis of the migrations is required to obtain fundamental characteristics of a sequestration structure, including estimation of its sequestration capacity and leakage risks. The paper presents a general discussion of the relevant mechanisms and their contributions to the analysed issues. The proposed approach to solve the problems relies on the usage of numerical structure modelling and simulations of the sequestration processes on numerical models of the structure. It is applied to a selected geological structure comprising a partially depleted gas reservoir. The modelling includes key types of reservoir fluid migrations: viscous multiphase transport and convection transport. It also takes into account other phenomena that affect fluid migrations including injected gas solubility in the formation water and gas trapping by capillary forces. Correspondingly, the leakage risks are associated with distinct leakage pathways (beyond the structural trap, to the caprock, via activated fractures). All these cases are separately modelled and their detailed characteristics are presented and discussed. The final results of the fluid migrations and their consequences for the leakage events are discussed and some generalized conclusions are drawn from the approach employed in the study.

Keywords: numerical modelling; reservoir simulations; reservoir fluid migrations; CO₂ sequestration; sequestration capacity; leakage risk analysis



Citation: Szott, W.; Miłek, K. Analysis of Reservoir Fluid Migration in the Process of CO₂ Sequestration in a Partially Depleted Gas Reservoir. *Energies* **2021**, *14*, 6398. <https://doi.org/10.3390/en14196398>

Academic Editors: Reza Rezaee and Pål Østebø Andersen

Received: 12 August 2021
Accepted: 25 September 2021
Published: 6 October 2021

Publisher's Note: MDPI stays neutral with regard to jurisdictional claims in published maps and institutional affiliations.



Copyright: © 2021 by the authors. Licensee MDPI, Basel, Switzerland. This article is an open access article distributed under the terms and conditions of the Creative Commons Attribution (CC BY) license (<https://creativecommons.org/licenses/by/4.0/>).

1. Introduction

The idea of gas sequestration such as CO₂ or other acid gases in geological structures is commonly considered a method of their utilization. A unique example of gas sequestration is given by the Borzęcin project described in [1–4]—the 25 year on-shore acid gas sequestration project. The study reported in this paper was performed on models of the Borzęcin structure.

Other long-lasting projects of the European contribution include the In Salah CO₂ Storage Project [5] and the Sleipner Carbon Capture and Sequestration Project [6]. Both of those projects are located at different geological settings: the In Salah Project has been reinjecting CO₂ into a fractured sandstone formation since 2004, the Sleipner Project has been reinjecting CO₂ to offshore sandstone formation since 1996. Hence, the Borzęcin Project is the longest-running on-shore sequestration project in Europe.

One of the most important aspects of CO₂ sequestration in deep geological structures refers to risks of CO₂ leakage to shallow geological formations or into the atmosphere which can damage the ecological system and caused hazards to human health. Detailed information about risk assessment procedures is presented in [7]. To assess leakage risks, it is necessary to study processes of fluid migrations within an analysed sequestration structure. There are several pathways of possible fluid migrations.

One of the most likely migration routes is to overburden rocks, which is governed by the threshold pressure. This parameter was extensively studied in experimental tests

under laboratory conditions in [8]. Field studies of the leakage path-ways to overburden rocks were performed in [9] but they were limited to the natural CO₂ reservoirs and did not refer to sequestration sites.

Other possible leakage path-ways are induced faults and/or fractures. These cases were studied by D. Alexander and D. Boodlal in [10]. They considered synthetic models of saline aquifers with faults characterized by features typical for potential sequestration structures in a selected geological area. Effects of fractures on gas migration were studied by S. Yang et al. in [11] for a case of enhanced shale gas recovery employing a numerical model based on geological data of Ordos basin in China. T. Nakajima et al. [12] performed numerical simulations of CO₂ leakage along fault system at a hypothetical CCS site with the fault/fracture parameters adopted from Tertiary formations in Japan.

J.R. Brydie et al. [13] recognized the potential leakage pathway via wellbores, which may provide a direct connection between the storage formation and the surface. They performed experimental studies to assess various potential blocking agents and conducted numerical simulations to assess the upscaling requirements of the blocking process in preparation for large-scale laboratory tests and a field demonstration. Their work proves a very complex dependence of the leakage via wellbores upon detailed parameters of the wellbore technicalities, cement bonding, and other characteristics of the wellbore construction. Analogous conclusions can be drawn from the studies by B. Doherty et al. [14] where they applied a special tool to estimate well leakage as response to different scenarios representing initial well states and configurations. Consequently, the problem of leakage via wellbores requires an individual approach to each and every well operating on a sequestration structure.

A significant leakage path-way can result from migrations of a sequestered gas beyond structural trap boundaries of the sequestration structure. This effect is a particular consequence of the injected gas plume evolution during the sequestration process. G. Zhang et al. [15] studied CO₂ plume migration and fate at Sleipner. They applied a multi-phase compositional simulation model to perform a sensitivity study of various simulation results, including plume migration, to changes of fundamental structure parameters. The problem of plume migration was a subject of the study by Y. Zapata et al. [16]. They investigated CO₂ plume characteristics and determined its evolution during a 100-year injection and 200-year post-injection periods in hypothetical saline aquifers. CO₂ plume migration was a subject of the studies by Y. Diao et al. [17] performed on the Shenhua CCS demonstration project in China. That project lasted only five years (2011–2015) and employed relatively shallow saline aquifers. None of the above studies took into account any leakage path-ways other than the one beyond structural trap boundaries.

In this paper we report on the studies of the reservoir fluid migration in the long-term running process of CO₂ sequestration in the structure of the Borzëcin partially depleted gas reservoir in the context of all possible leakage pathways with the exception of leakage via wellbores, as justified above.

To this aim we employed numerical modelling of the analysed structure and simulations of the migration processes performed on the model that was calibrated against the data of 25-years' sequestration history. In general, the modelling of CO₂ sequestration in deep geological structures was performed by many groups of investigators. Such modelling may be exemplified by E.J. Mackay [18], C. Khan et al. [19], W. Szott et al. [20]. They investigated general aspects of CO₂ sequestration with possible anticipatory CO₂ enhanced gas recovery and did not study reservoir fluid migrations in the context of CO₂ leakage risks.

The model of the analysed sequestration structure was constructed and calibrated as reported in the authors' previous publications [21,22]. This paper presents an application of the existing model and its necessary extensions to analyse reservoir fluid migrations and their potential leakage via three typical leakage pathways listed above. Particular tasks concerning statistical analysis presented below were performed according to conventional computer-assisted approach [23].

The approach applied in this study does not include a coupled dynamical and geomechanical simulations, i.e., assumes small influence of the variation of geomechanical state upon the transport properties of the structure rocks. The detailed analysis of this problem is a subject of other papers by the authors. The first paper concerning the subject is [24] Other papers on this subject are in preparation.

The uniqueness of the study presented in this paper refers to: (i) a unique sequestration project of 25 years' history—that infers large amount of operational and monitoring data; (ii) a most complete analysis of fluid migrations including various leakage path-ways.

2. Reservoir Fluid Migrations

Significant consequences of reservoir fluid migrations during the process of gas sequestration are given by potential leakage risks outside the sequestration site. There are commonly identified as four leakage risk factors according to the following leakage pathways:

- leakage beyond the structural trap,
- leakage to the caprock by exceeding caprock threshold pressure,
- leakage along activated fractures or other rock discontinuities,
- leakage along well trajectories (deterioration of well integrity).

The first one occurs when the plume of the injected fluid migrates along the spill trajectories out of the geological structure boundaries defined by caprock local depressions. This case refers to both free phase of the injected fluid and its aqueous solution.

The second one occurs across the reservoir-caprock boundary to overburden rocks. The sealing properties of the caprock are determined primarily by the capillary threshold pressure, which arises from a pore pressure step across the reservoir-caprock boundary for primary pressure vertical distribution. For obvious reasons the actual threshold pressure is not lower than the pressure step at the highest point of the reservoir-overburden boundary.

During the process of gas sequestration in a target structure, a local pore pressure may exceed formation breakdown (fracturing) pressure that is an important characteristic of the structure rock properties. As a consequence, either original fractures can be generated or existing but closed fractures can be opened. If such fractures extend up to the structure overburden, they provide conductive channels for the injected fluid to escape from the sequestration structure.

The last leakage pathway can occur when the integrity of an injecting or monitoring well is deteriorated due to variety of reasons such as failed cement bonding or its erosion. Contrary to the previous three leakage pathways, this one depends upon the technical state of wells and specific geomechanical state of the wells and surroundings and therefore cannot be forecasted prior to well completions.

Analysis of the reservoir fluid migrations resulting in potential leakage events can be obviously performed with the application of numerical structure modelling and simulations of various key reservoir processes taking place during gas sequestration projects. This approach may be realised in both feasibility studies, monitoring, and long-term relaxation phases of such projects. Its basic result includes estimations of the analysed structure sequestration capacity defined as maximum total injection volume avoiding leakage events.

The sequestration capacity strongly depends upon various groups of factors. The first one includes reservoir and fluid properties:

- geological properties of the structure (size and shape of structural trap, effective pore volume, absolute permeability and its anisotropy, formation breakdown «fracturing» pressure, caprock threshold pressure, reservoir water distributions, reservoir temperature and pressure, presence, and activity of surrounding and underlying aquifers),
 - thermodynamic state of reservoir fluids (single-phase vs. multi-phase state, interphase tension),
 - transport properties of the original reservoir fluid and its mixture with injected CO₂ (miscible vs. immiscible displacement, effective phase permeabilities),
 - other properties (CO₂ solubility in water, CO₂ reactivity with rock minerals).
- The other includes operation and technical parameters of a sequestration project:

- number and location of injection wells,
- depth of completion intervals (relative to the reservoir fluid distribution),
- contribution of injection wells in a total injection stream,
- injection rates.

The rest of the paper presents the application of the numerical modelling and simulation approach to an example of a geological structure primarily containing a reservoir natural gas that is partially depleted.

3. Structure Modelling

The analysed geological structure includes the natural gas field located in the southern part of the Pre-Sudetic Monocline, Poland [21]. It forms an anticline with two local uprisings. The structure includes the Zechstein anhydrites and salt formation over the Basal limestone formation on top of the Rotliegend sandstone formation. The Basal limestone horizon and the Rotliegend sandstone horizon are hydrodynamically connected while the Zechstein horizon forms a caprock of the former. The natural gas zone is limited by the underlying water.

A simulation model of the structure was constructed and calibrated [21]. A geological model was generated based on standard input data including structural maps of the above listed formations. An example of the structural map of the Basal limestone top is shown in Figure 1 that also defines a vertical cross section line A–A'.

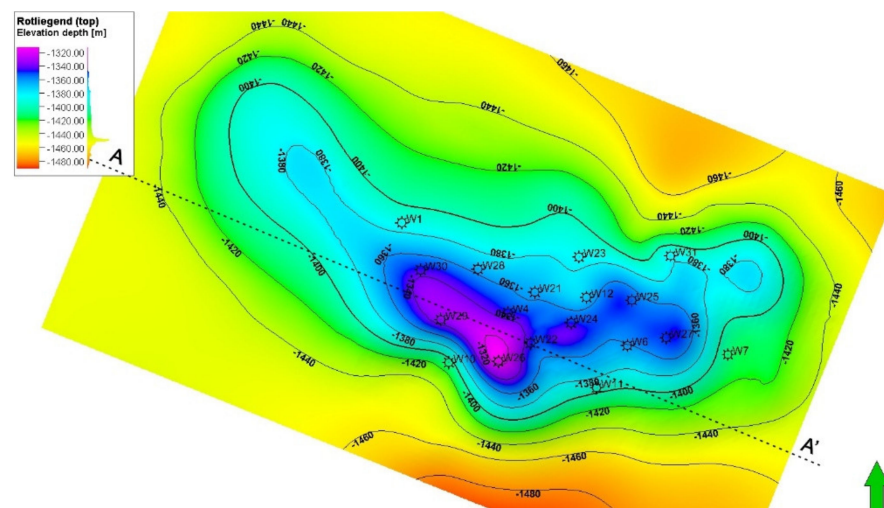


Figure 1. Structural map of the reservoir top. Location of line A–A'.

A basic parametric model of the structure was constructed based on standard input data sources including geophysical logs, laboratory measurements of well core samples, etc. Those data were used to generate lithological, stratigraphic, and geophysical structures for all tested wells. For spatial distributions of key geological parameters (porosity, permeability, net-to-gross thickness ratio), a variographic analysis was applied. The resulting variogram (spherical type) and its parameters (sill, range values) were used to conditionally simulate (by sequential gaussian simulation) stochastic realizations of all parameter distributions [25]. The effects of fine-scale features [26] and their influence on rock deformations [27] were considered as those of higher order and postponed to future studies. Final distributions of the geological parameters were obtained by averaging 20 of those realizations. Figures 2–4 present these distributions as vertical cross sections along A–A', planar distributions of porosity at the Basal limestone top and Rotliegend bottom, and permeability distribution at the Basal limestone top and Rotliegend bottom, respectively.

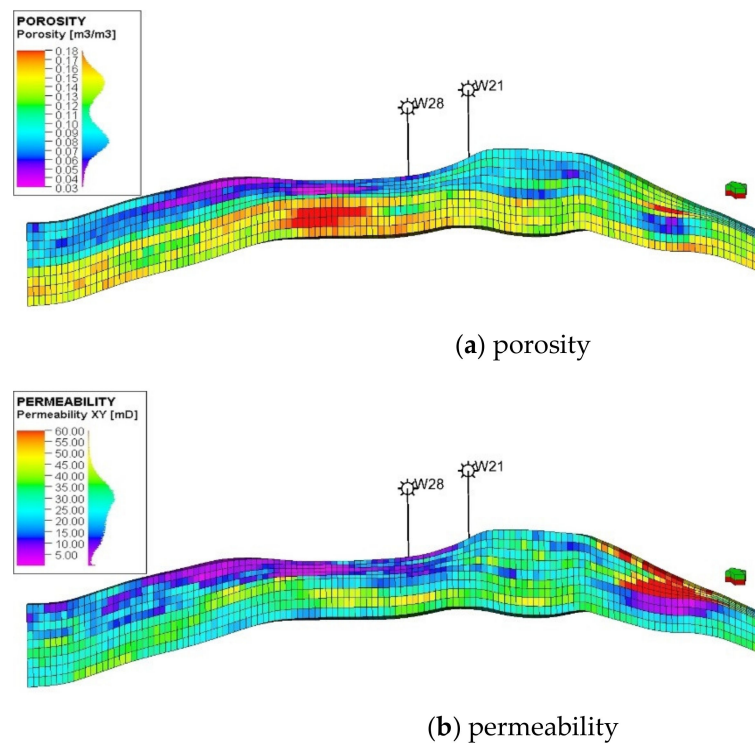


Figure 2. Porosity and permeability distributions along the vertical cross section (A–A’).

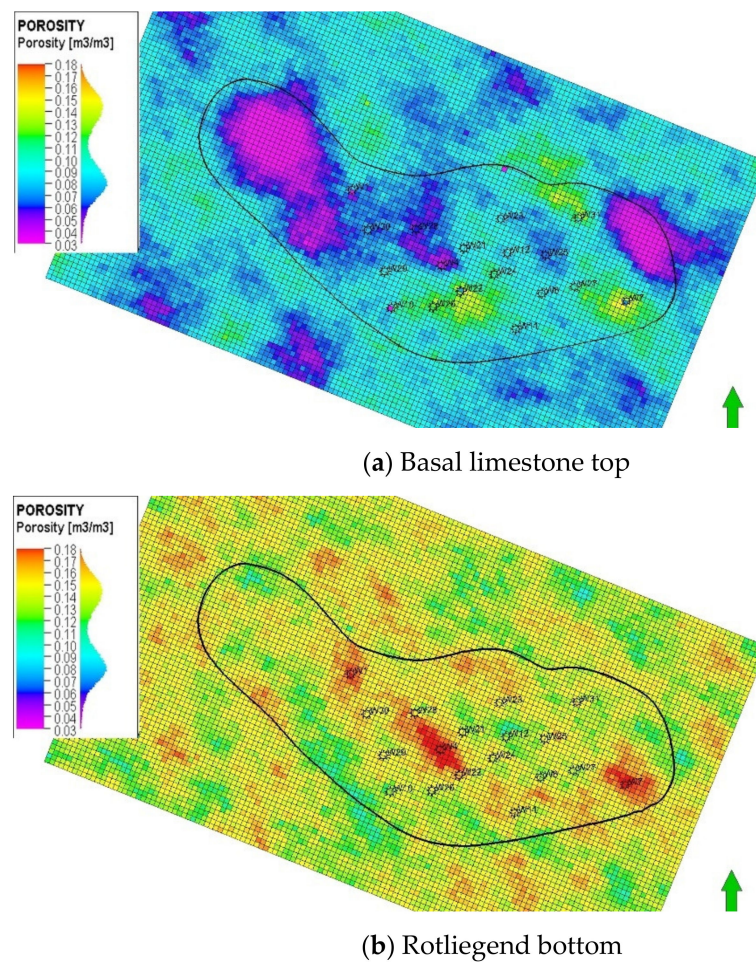
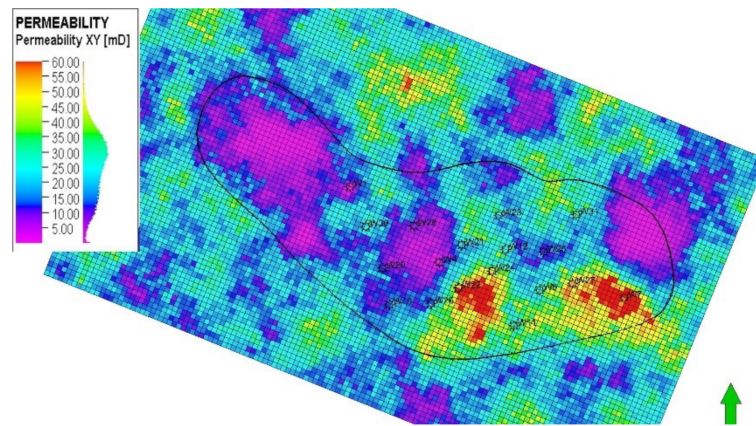
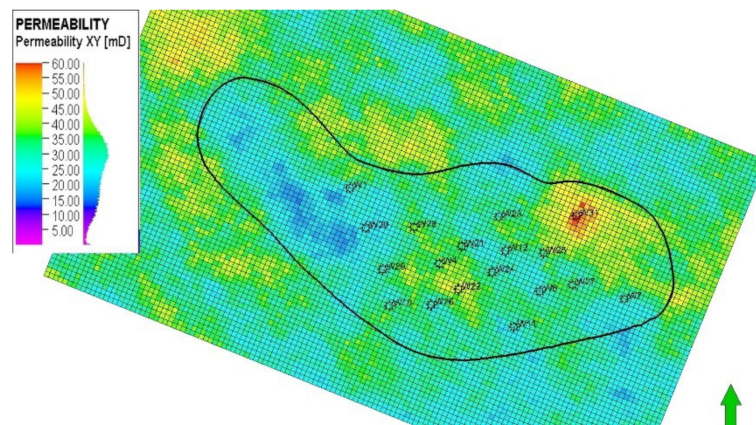


Figure 3. Porosity distribution at Basal limestone top and Rotliegend bottom.



(a) Basal limestone top



(b) Rotliegend bottom

Figure 4. Permeability distribution at Basal limestone top and Rotliegend bottom.

Based on the geological model a dynamical simulation model of the structure was constructed [19] that included the original gas-bearing zone surrounded by an active water-bearing zone.

The dynamical model was complemented with initial gas and water saturation distributions consistent with measured data and complying hydrostatic conditions and an original water-gas contact depth. Resulting gas saturation distribution is presented in Figures 5 and 6.

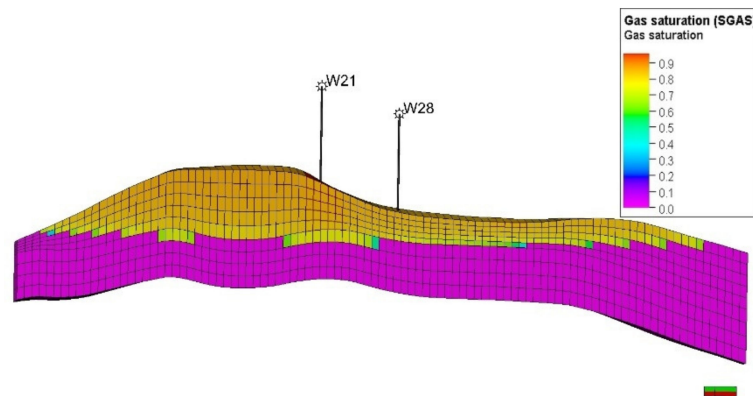


Figure 5. Original gas saturation distribution along the vertical cross section (A–A’).

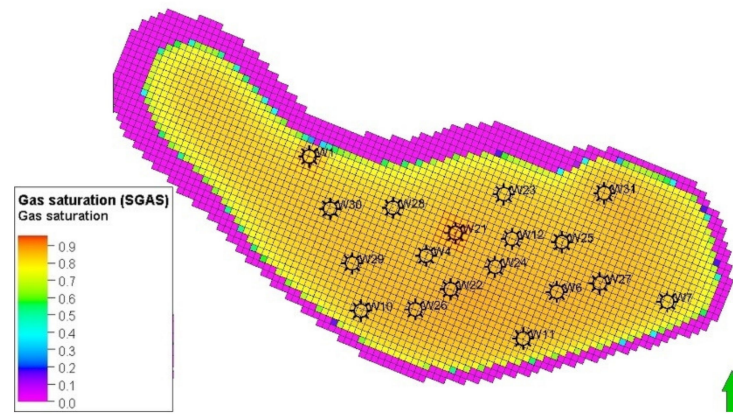


Figure 6. Original gas saturation distribution at the Basal limestone top.

A standard Corey type dependences upon fluid saturations were adopted for relative permeabilities used in the model.

The simulation model of the analysed structure was formulated as a compositional one for the variations of the reservoir gas composition to be reconstructed and monitored. To this aim the Peng-Robinson equation of state and standard Lorentz-Bray-Clark viscosity correlation were applied and six parameter (three hydrocarbon components: C₁, C₂, C₃₊, and three nonhydrocarbon components: N₂, CO₂, H₂S) gas composition was assumed. The initial gas composition is given in Table 1.

Table 1. Composition of original gas.

Component	Mole Fraction
N ₂	0.3630
CO ₂	0.0028
H ₂ S	0.0013
C ₁	0.6110
C ₂	0.0197
C ₃₊	0.0046

Reservoir brine properties applied in the model consist of: density (1100 kg/m³), salinity (150 g/L), formation volume factor: (1.011 Rm³/Sm³ @ 154.8 bar, 46.8 °C), compressibility (4.5 × 10⁻⁵ 1/bar), viscosity (0.66 cP, @ 154.8 bar, 46.8 °C), viscosibility (6 × 10⁻⁵ 1/bar).

In addition, CO₂ solubility in the reservoir brine was taken into account based on the laboratory measurements [28] shown together with interpolating curves in Figure 7.

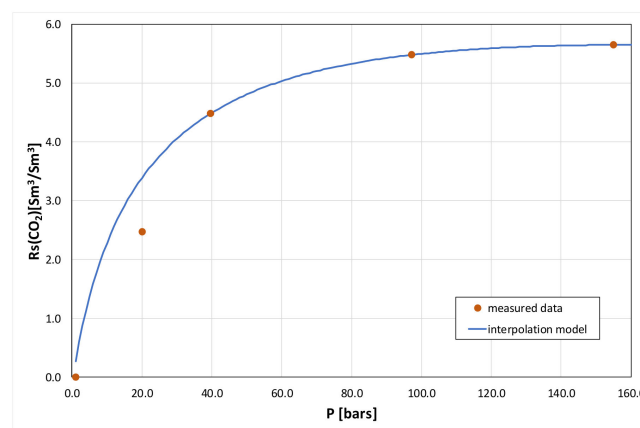


Figure 7. CO₂ solubility in the reservoir brine vs. pressure at the reservoir temperature.

The dynamical model was complemented with basic well data (localizations, trajectories, radii, completion intervals). The complete model of the structure used the format of Eclipse simulator by Schlumberger®.

The simulation model of the structure was calibrated based upon the gas reservoir operational data [4]. Examples of the calibration results are given in: Figures 8–10 as bottomhole pressures, water-gas ratios, and CO₂ concentrations of the produced gas in Well W4, respectively.

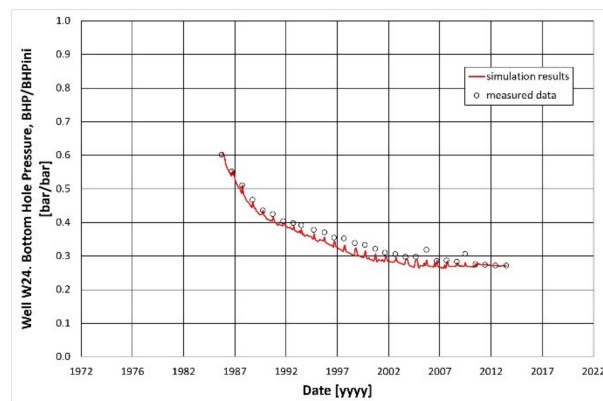


Figure 8. Results of model calibration. Measured bottom hole pressure vs. simulation results. Well W24.

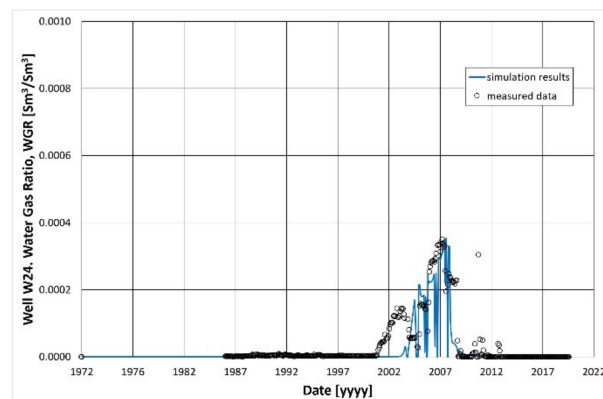


Figure 9. Results of model calibration. Measured water-gas ratio vs. simulation results. Well W24.

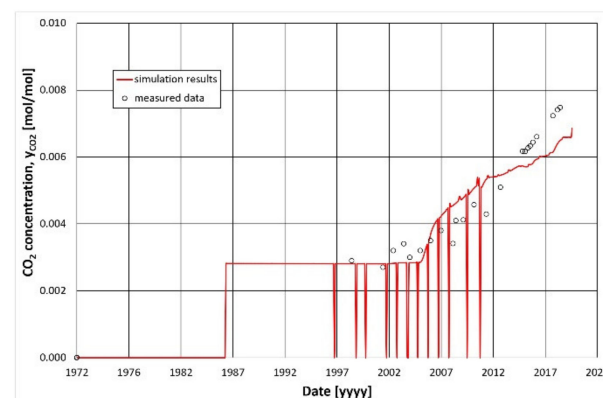


Figure 10. Results of model calibration. Measured CO₂ concentration in produced gas vs. simulation results. Well W22.

The calibration process concluded with a satisfactory match of the model results to the measured data and resulted in several modifications of model parameters including: the division of the model into three partially separated regions (western, central, and eastern ones as shown in Figure 11) required to match three different measured pressure trends as presented in Figure 12; transmissibilities between these regions; their effective pore volumes; characteristic parameters of underlying aquifers; global vertical to horizontal permeability anisotropy; local transport properties in several well drainage zones.

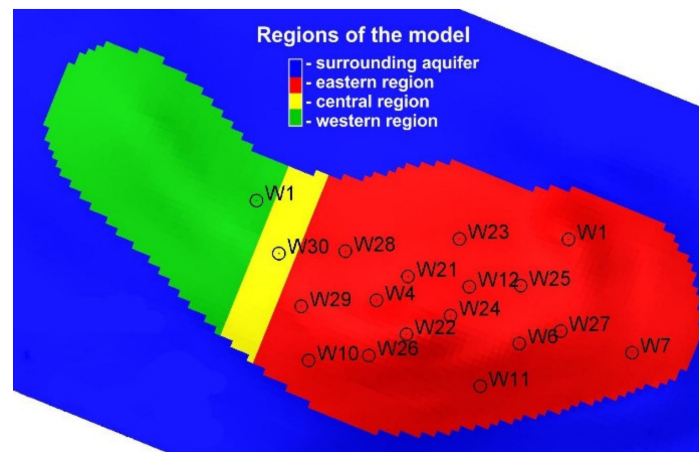


Figure 11. Top view of the reservoir simulation model with definitions of partially isolated reservoir regions and surrounding aquifer.

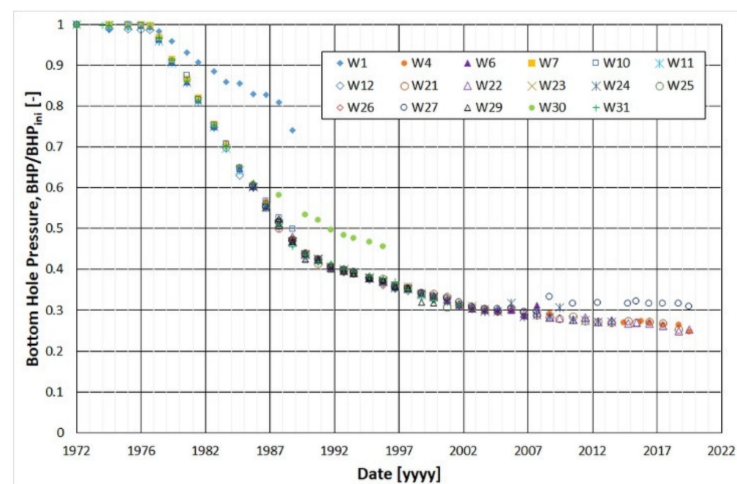


Figure 12. Bottomhole pressure of producing wells. Three trends identified as indicated by: (1). W1, (2). W30, (3). the other wells: W4, W6, W7, W10–W12, W21–W27, W29, W31.

4. Sequestration Capacity

The calibrated model of the structure is used for the detailed analysis of processes taking place during the sequestration project resulting, among others, in the estimation of the sequestration capacity. This value depends upon and requires the adoption of several technical assumption of the sequestration project. The key assumption refers to the well system applied to the injection phase of the project. For the analysed structure the well system includes 17 wells shown in Figure 13.

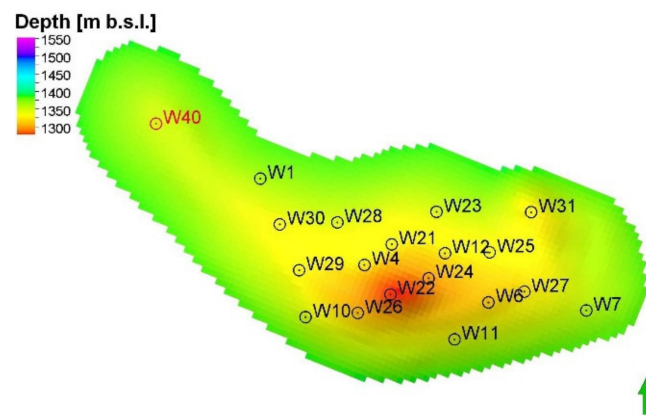


Figure 13. Location of injection wells of the analysed structure.

Additional assumptions include:

- completion of the injection wells in aquifers underlying the gas cap,
- maximum injection rates of an individual well, $q_{g,inj,max} = 400,000 \text{ Nm}^3/\text{d}$,
- maximum bottomhole injection pressure, $P_{bhp,max} = 200 \text{ bar}$.

While fulfilling these assumptions, varying total CO₂ injection scenarios were tested against the following risk determinants:

- no leakage of the injected CO₂ beyond the structural trap,
- maximum pressure in the structure volume below the formation damage (fracturing) pressure,
- maximum pressure step across the reservoir-caprock boundary below the displacement threshold pressure.

The scenarios differ in injection schedules and in contributions of the individual injection wells to the total injection stream. As a result of the optimization process taking into account the above criteria, a simulation scenario was determined for which the amount of CO₂ injected into the structure was maximized. Thus, the sequestration capacity was found to be 135% of the OGIP (original gas in place) and the injection phase lasted 8 years and 5 months.

The maximum local pressure was localized along the trajectory of an injection well. Its value was 108% of the initial pressure in the reservoir and was significantly lower than the fracturing pressure of the structure rocks. Therefore, there is no risk of gas leakage through the fracture into the overburden.

Another risk factor for gas leakage related to the displacement threshold pressure was analysed by the estimation of the pressure step across the reservoir-caprock boundary that reached its maximum value at the end of the injection phase and at the highest point of the structure and did not exceed the threshold pressure.

5. CO₂ Sequestration Forecasts vs. Total Injection

Additional scenarios were performed to study the effects of increased total injection upon the sequestration process. In general, total injection volumes exceeding the sequestration capacity resulted in violating any of the three leakage criteria related to and listed in the “Leakage pathways” chapter above. Below, the three cases were studied separately, one at a time.

The case of the leakage beyond the structural trap boundaries was investigated in four scenarios differing in the total injection volumes relative to the sequestration capacity found earlier. Figure 14 shows the leakage volume as a function of time for the scenarios of the total injections equal to 128%, 154%, 180%, and 205% of the sequestration capacity for the subsequent four scenarios respectively. It is worth noting that leakage prolongs a long time (up to 100 years) after the injection phase is finished. The amount of total leakage

after 100 years was 0.002%, 0.06%, 0.42%, 1.25% of the sequestration capacity CO₂ volume, for the four scenarios, respectively.

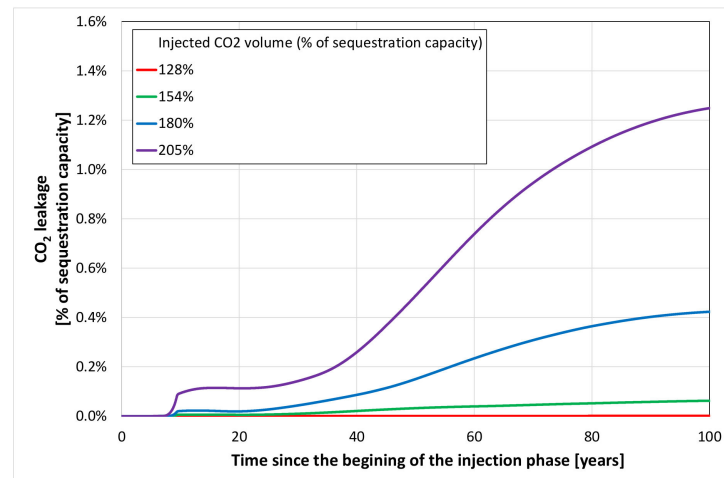


Figure 14. CO₂ leakage beyond the structural trap vs. time.

The size of the leakage and its time evolution were influenced by:

- increased total injection volume and, consequently, an increased pressure difference across the storage zone and surrounding water-bearing horizons causes the migration of the injected CO₂ in the free phase beyond the trap boundaries,
- equalization of gas saturations (flows inside the storage zone) in the relaxation phase with a simultaneous slow pressure drop in some regions due to the pressure equalization process (and a consequent decrease in the amount of CO₂ dissolved in the brine) increases the volume of the mobile gas that migrates beyond the trap boundaries.

Further analysis of the total CO₂ leakage beyond the trap boundaries as a function of the storage capacity filling for $t = 10, 50, 100$ years since the injection start (Figure 15) allowed to formulate the following conclusions:

- the amount of the total leakage significantly increases in cases where more than 154% of the sequestration capacity has been injected,
- in the case of the total injection volume up to 154% of the sequestration capacity, the rate of CO₂ leakage from the storage zone does not vary with time,
- in the case of the total injection volume above 180% of the sequestration capacity, most of the outflow beyond the trap boundaries occurs in the first 50 years, when a high-pressure difference is observed between the storage zone and the surrounding aquifers.

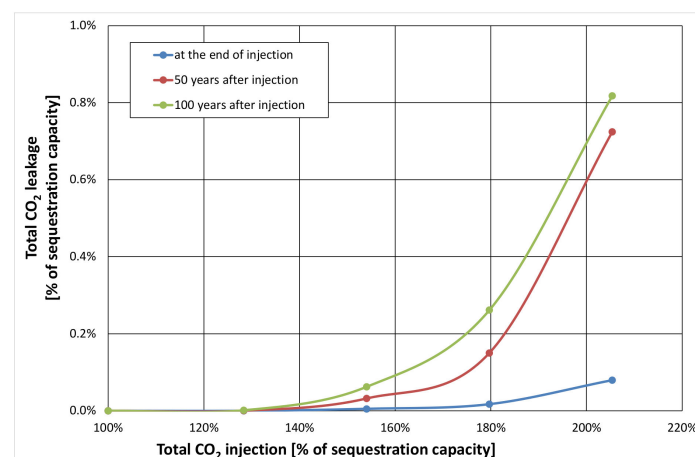


Figure 15. Total CO₂ leakage beyond the structural trap as a function of total injection.

The identification of the sites where gas leaks beyond the storage zone is available with the analysis of free-phase gas saturation in the top layer of the storage zone and in vertical sections of the structure. An example of data for such an analysis is presented in Figure 16 for the scenario in which the total injection volume equals 205% of the sequestration capacity. From these data it can be concluded that during the injection phase of the sequestration project the leakage beyond the storage zone occurs near the wells, i.e., in the south-eastern part of the reservoir, and then during relaxation phase of the sequestration project—along quite different routes i.e., in the northern, north-western and south-western parts of the reservoir.

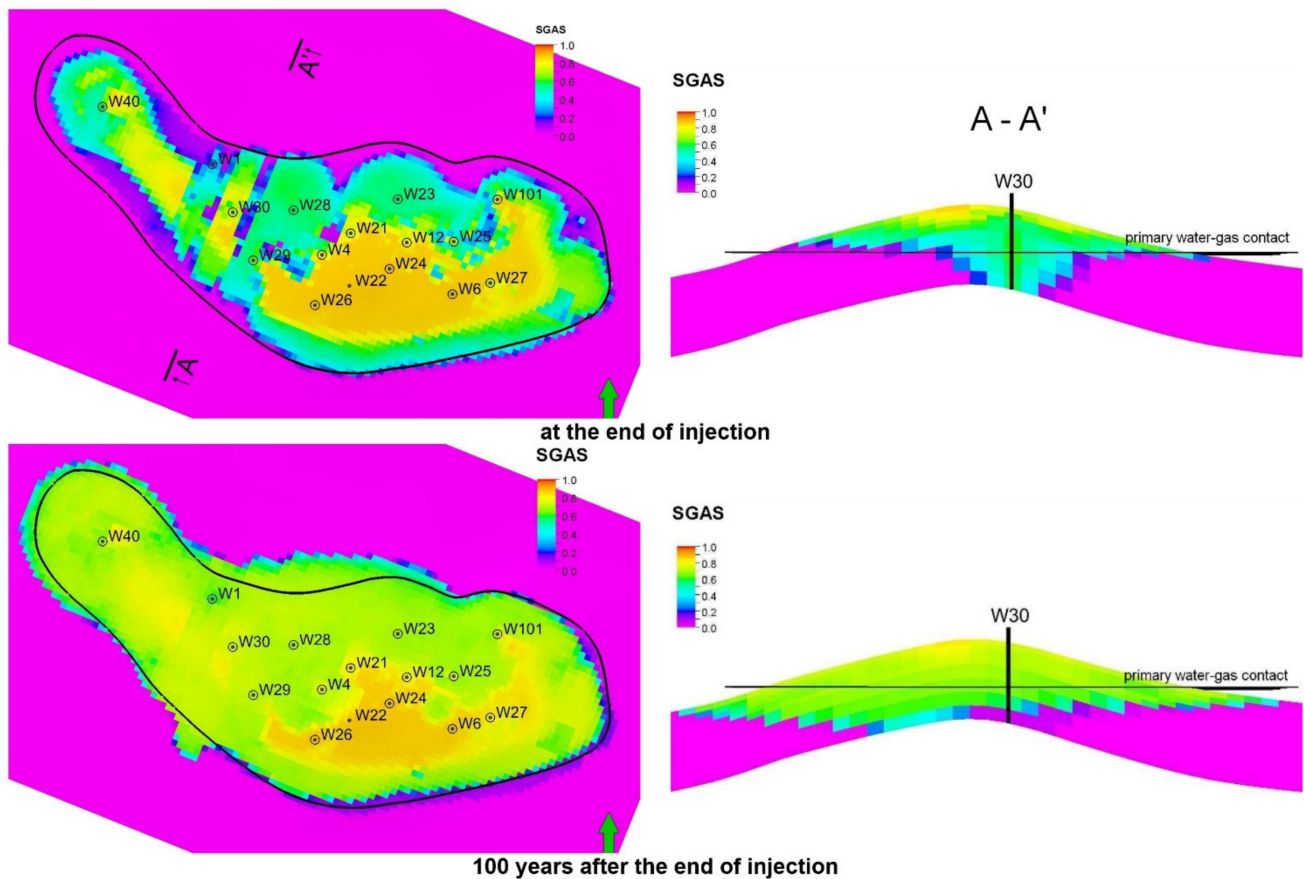


Figure 16. Injection gas (CO_2) saturation distribution in the top layer and on the vertical section along the A–A' line for total injection, $G_{\text{inj}} = 205\%$ of the sequestration capacity.

This analysis not only allows to identify the most critical places of potential gas leakage but also to optimize the contribution of individual wells to the total injected gas stream to reduce the leakage.

Below, the simulation of the other two leakage paths are presented and discussed in detail. The dimensionality of the models applied to simulate them was selected the smallest ones that are sufficient to model each of them. Therefore, it is a 1D model for leakage to the caprock by exceeding threshold pressure and a 2D model for leakage via a fracture.

6. 1D Model of CO_2 Migration in the Overburden Due to Exceeding Displacement Threshold Pressure

In order to investigate processes of injected gas leakage to the overburden and to estimate leakage quantities, a one-dimensional simulation model was applied taking into account detailed characteristics of the overburden.

For these purposes, a high-resolution 1D model was constructed including a storage zone together with an extended overburden zone (with the total thickness above 1000 m) including anhydrite and rock salt horizons as shown in the most left part of Figure 17. The detailed parametric model was based upon the stratigraphic data presented in Table 2.

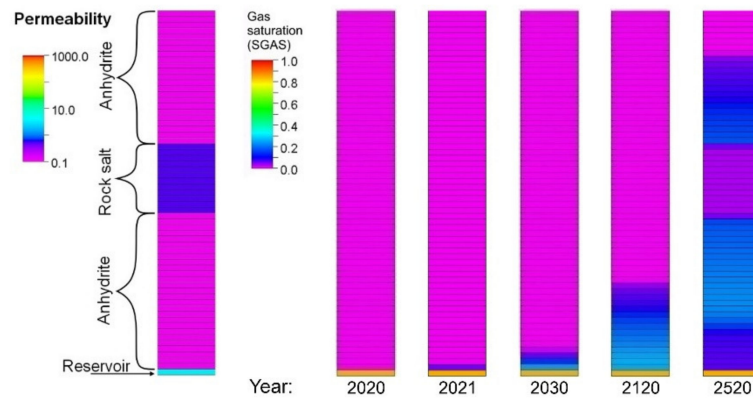


Figure 17. CO₂ migration to the overburden rocks. Distribution of CO₂ saturation as a function of time. Basic scenario for constant formation pressure, Pres = 170.68 bar.

Table 2. Stratigraphic table containing the division into separate layers with variable properties in overburden and reservoir series.

No.	Thickness	Top TVDSS	Bottom TVDSS	Model Element	Stratigraphy	Porosity [%]	Permeability [mD]
1	340.0	−90.0	250.0	Overburden	Quaternary + Tertiary + Lower Keuper + Upper Muschelkalk	15.00	50
2	0.0	250.0	250.0		Lower Keuper	12.60	144
3	0.0	250.0	250.0		Upper Muschelkalk	15.00	350
4	45.0	250.0	295.0		Middle Muschelkalk	15.00	350
5	155.0	295.0	450.0		Lower Muschelkalk	15.00	350
6	129.0	450.0	579.0		Upper Bunter Sandstone—ret	15.00	100
7	215.0	579.0	794.0		Middle Bunter Sandstone	15.00	100
8	305.0	794.0	1099.0		Lower Bunter Sandstone	15.00	100
9	21.0	1099.0	1120.0		Transitional Claystones	1.50	0.0005
10	0.0	1120.0	1120.0		Youngest Halite—Na4b2	1.50	0.0005
11	0.0	1120.0	1120.0		Lower Red Pelite—T4a	1.50	0.0005
12	15.0	1120.0	1135.0		Younger Halite—Na3	1.50	0.0005
13	32.0	1135.0	1167.0		Main Anhydrite—A3	1.50	0.0005
14	3.0	1167.0	1170.0		Gray Pelite—T3	1.50	0.0005
15	25.0	1170.0	1195.0		Basal Anhydrite—A2	1.50	0.0005
16	15.0	1195.0	1210.0		Main Dolomite—Ca2	15.00	200
17	39.0	1210.0	1249.0		Upper Anhydrite—A1g	1.50	0.0005
18	6.0	1249.0	1255.0		Oldest Halite—Na1	1.50	0.5000
19	13.5	1255.0	1268.5		Lower Anhydrite—A1d	1.50	0.0005
20	76.0	1268.5	1344.5	Zechstein Limestone—Ca1	9.12	3.7043	
21	0.0	1344.5	1344.5	Reservoir	Kupferschiefer	1.50	0.0005
22	30.5	1344.5	1375.0		Rotliegendes	14.85	8.8547

The model adopted the estimated displacement threshold pressure of the caprock ($P_{th} = 9.25$ bar). Two ensembles of several scenarios each were investigated differing in initial pressures at the storage zone top corresponding to various exceeding of the threshold pressure and in the pressure, boundary conditions at the storage zone top—this pressure was either kept constant or naturally decreasing according to the steady depletion of the

storage zone by the leakage effects. The ensemble no. 1 included scenarios with the storage zone initial pressure of $P_{ini1,s} = 165.68$ bar, which is equivalent to exceeding the threshold pressure by 12 bar. The Ensemble no. 2 included scenarios with the storage zone initial pressure of $P_{ini1,s} = 170.68$ bar, which is equivalent to exceeding the threshold pressure by 17 bar. An example of simulation results in terms of a leaked gas distribution across the overburden for a scenario from the Ensemble no. 2 is shown in Figure 17. Similar results were obtained for other scenarios of this ensemble and they will be presented and discussed below. Results in Figure 17 are described below:

- during gas migration through the anhydrite, the main factor determining the relatively small migration velocity is the low absolute permeability of the rock,
- a secondary factor affecting the velocity of the gas migration is the pressure at the top of the storage zone (the bottom of the overburden),
- during gas migration through the anhydrite, it reaches saturation, $S_g \sim 26\%$, which determines its effective phase permeability,
- after reaching the rock salt horizon, gas migration is faster due to their larger absolute permeability,
- in the rock salt horizon, gas migration becomes effective at relatively low gas saturation due to small critical gas saturation $S_{gcr} = 10\%$,
- decrease of gas saturation in the anhydrite formations to the value of $S_g \sim 18\%$ after 500 years since the end of injection results from the fast migration of gas through the rock salt horizon and the decrease of the pressure at the top of the storage zone.

7. Ensemble Approach to Study CO₂ Migration in the Overburden of Uncertain Properties

Since the main parameters of the overburden rocks, such as the absolute permeability of young rock salts and anhydrite (YRS&A—rocks with relatively low permeabilities), and the old rock salts (ORS—rocks with relatively high permeability) were known with high uncertainty, therefore an ensemble approach was applied to study the influence of these parameters upon the results of leaked gas migration in the overburden. The uncertain parameters were assumed to vary within a selected range of values for a selected probability distribution. The list of these parameters include:

- absolute permeability of young rock salts and anhydrite (YRS&A),
- absolute permeability of old rock salts (ORS),
- maximum gas relative permeability (K_{rgmax}),
- critical saturation for gas (S_{gcr}),
- critical saturation for water (S_{wcr}),
- threshold pressure (P_{th}).

The first two parameters were modified by multiplicative factors: MF_YRS&A and MF_ORs for YRS&A and ORs, respectively, and their probability distributions were of logarithmic-triangular type. The remaining parameters were directly modified with triangular probability distributions. The detailed data of the parameter reliability are given in Table 3.

Table 3. Table of parameters variability to generate the ensembles.

Parameter	Distribution of Parameter Variability	Value		
		Min	Median	Max
MF_YRS&A	log-triangular	−0.301	0.000	0.301
MF_ORs	log-triangular	−0.301	0.000	0.301
K_{rgmax}	triangular	0.400	0.700	1.000
S_{gcr}	triangular	0.050	0.100	0.200
S_{wcr}	triangular	0.200	0.300	0.400
P_{th}	triangular	9.249	9.250	14.250

Based on the assumed variability of input parameters and the initial pressure at the bottom of the underburden two ensembles were generated with the multiplicity of $n = 729$ cases (scenarios).

Basic simulation results of the ensemble cases in the form of CO₂ leakage as function of total injection volume (related to the sequestration capacity) for Ensemble no. 1 ($P_{ini1,s} = 165.68$ bar) is the amount of leakage after 500 years from the end of gas injection. It ranges from 0.13% to 0.40% of sequestration capacity, while for Ensemble no. 2 ($P_{ini2,s} = 170.68$ bar), the amount of leakage ranges from 0.23 to 0.55% (Figure 18).

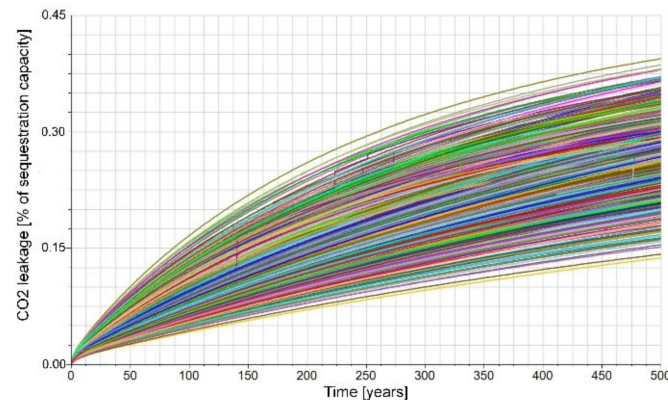


Figure 18. CO₂ leakage into the overburden vs. time. Ensemble no. 2.

For the above forecasts, a distance of the gas front position from the overburden bottom ranges from 9 to 33 m (for Ensemble no. 1 with initial pressure $P_{ini1,s} = 165.68$ bar at the bottom boundary of the overburden). The same quantity varies between 12 and 39 m for Ensemble no. 2 with initial pressure $P_{ini2,s} = 170.68$ bar as shown in Figure 19.

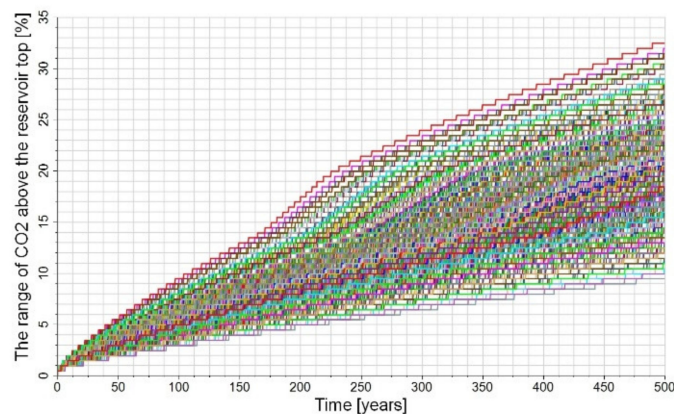


Figure 19. The distance of CO₂ migration in the overburden vs. time. Ensemble no. 2.

Step-like variation of the distance results from the finite resolution (0.5 m) of the model vertical structure.

The statistical analysis for both ensembles is presented in Figures 20 and 21 for CO₂ leakage and distance of CO₂ migration in the overburden, respectively. It contains histograms of the results discussed above together with their cumulative distribution functions of the simulation results after 500 years from the end of gas injection. Based on these results the following conclusions can be made:

- both the values of the total CO₂ leakage and the distances between the gas front position from the overburden bottom are smaller for Ensemble no. 1 ($P_{ini1,s} = 165.68$ bar) than those for Ensemble no. 2 ($P_{ini2,s} = 170.68$ bar),
- the scatter of the results for Ensemble no. 1 ($P_{ini1,s} = 165.68$ bar) is also smaller than the one for Ensemble no. 2 ($P_{ini2,s} = 170.68$ bar),

- the difference of the results for the distances between the gas front location and the overburden bottom between the two ensembles is smaller than the analogous difference of the results for the total leakage between the two ensembles.

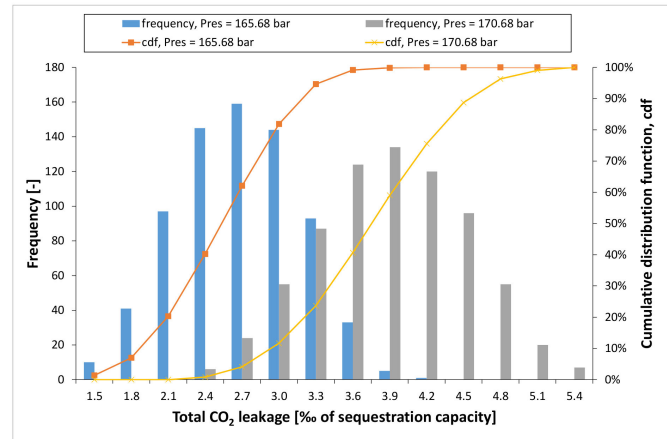


Figure 20. Histogram of the total CO₂ leakage to the overburden 500 years after the end of injection for Ensemble no. 1 ($P_{ini1,s} = 165.68$ bar) and Ensemble no. 2 ($P_{ini2,s} = 170.68$ bar).

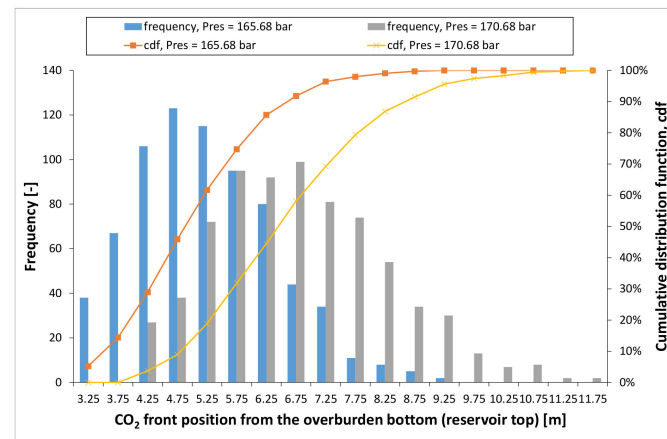


Figure 21. Histogram of CO₂ front position from the overburden bottom 500 years after the end of injection for Ensemble no. 1 ($P_{ini1,s} = 165.68$ bar) and for Ensemble no. 2 ($P_{ini2,s} = 170.68$ bar).

8. 2D Model of CO₂ Migration in the Overburden via Induced Fractures

The last case of the CO₂ migration in the overburden refers to CO₂ leakage via induced fractures. For the study of this migration 2D models of the structure vertical cross-section were constructed with vertical resolution of 0.5 m. The data from Table 2 were implemented into the parametric model with a uniform distribution in horizontal layers. Figure 22 presents a detailed layer structure of the overburden used in the 2D model for this case.

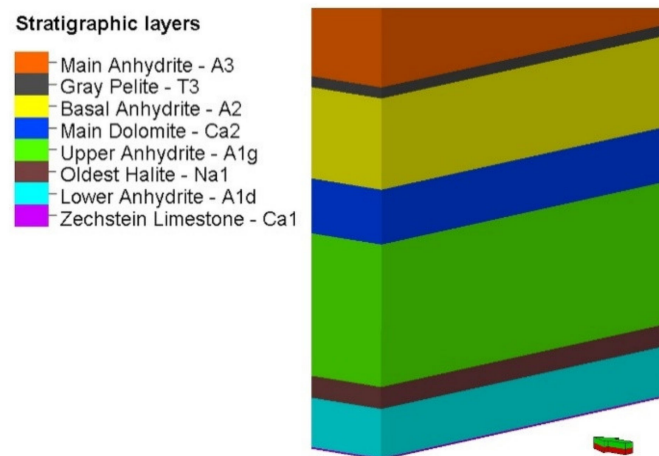


Figure 22. Layer structure of the overburden.

For the purposes of studying the gas migration to the overburden within induced macro-fractures, three simulation models were constructed. They differed in the properties of a macro-fractures as follow:

- Model I with infinite conductivity fracture and constant pressure at the reservoir top/overburden bottom over time,
- Model II with finite conductivity fracture and constant pressure at the reservoir top/overburden bottom over time,
- Model III with finite conductivity fracture and naturally decreasing pressure at the reservoir top/overburden bottom according to the steady depletion of the storage zone by the leakage effects.

For each of the above models, the initial pressure at the reservoir top/overburden bottom was assumed to be, $P_{ini} = 170.68$ bar.

Another unknown factor that was used in scenario of the models described above was the height of the resulting fracture. For the sake of simplicity, it was assumed that the fracture is formed in the entire thickness of separated formations, therefore, for each model, three Sub-scenarios were considered where the induced fracture extends up to:

1. lower anhydrite (LA),
2. lower anhydrite + old rock salt (LA + ORS),
3. lower anhydrite + old rock salt + upper anhydrite (LA + ORS + UA).

The rates and total CO₂ leakage volumes to the overburden rocks obtained as results of the simulations on the above Model I are presented in Figures 23–25 for Sub-scenario 1, Sub-scenario 2, and Sub-scenario 3, respectively. These results can be summarized as follow:

- for the shortest fracture (Sub-scenario 1) its conductivity does not affect the rate and total leakage volume, while for the longer fractures (Sub-scenario 2 and Sub-scenario 3), the larger the conductivity the larger the leakage,
- for Model III (assuming a decrease of the pressure at the reservoir top/overburden bottom according to the steady depletion of the storage zone by the leakage effects) the outflow rate decreases with time due to the ever-lower pressure gradient between the fracture and the overburden,
- for Models I and Models II (assuming constant pressure at the reservoir top/overburden bottom over time) the leakage rate decreases for the first 70 years (LA fracture), while in the following years the leakage rate begins to increase, which is related to the movement of the gas front, resulting in an increase in gas saturation in subsequent layers, and which in turn causes an increase in phase permeability for gas (resistance drop),
- for the shortest fracture (Sub-scenario 1), its conductivity does not affect the results, while in the case of further extending fractures (Sub-scenario 2 and Sub-scenario 3)

their conductivities have significant impacts on the leakage rate which increases with the fracture extension.

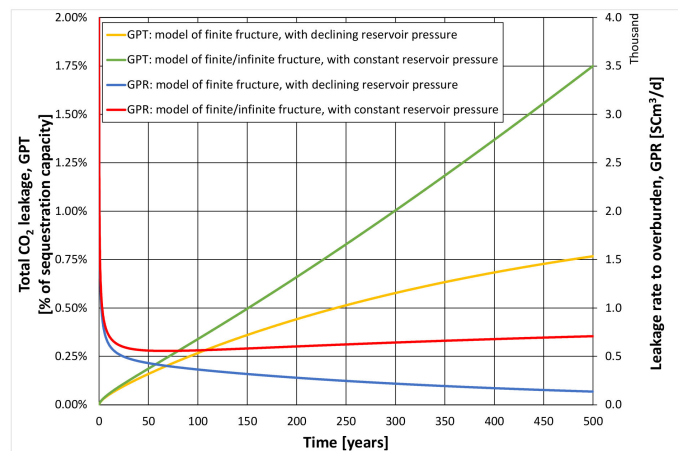


Figure 23. Rate and total CO₂ leakage to overburden. Scenarios for different fracture models and pressure conditions. Fracture range: lower anhydrite.

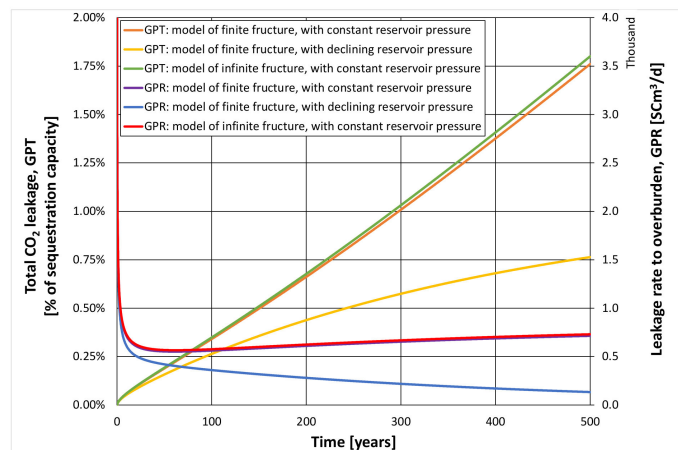


Figure 24. Rate and total CO₂ leakage to overburden. Scenarios for different fracture models and pressure conditions. Fracture range: lower anhydrite + old rock salt.

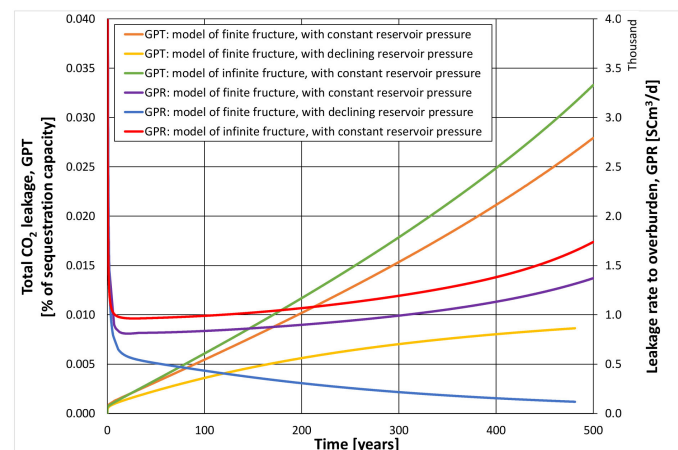


Figure 25. Rate and total CO₂ leakage to overburden. Scenarios for different fracture models and pressure conditions. Fracture range: lower anhydrite + old rock salt + upper anhydrite.

The detailed analysis of gas migration in the overburden due to the gas leakage from the sequestration zone via an induced fracture is based upon the studies of the evolution of gas distributions obtained from the simulation predictions performed on three models introduced above. As an example, the results of Sub-scenario 3 (for the longest-range fracture extended across lower anhydrite, old rock salt, and upper anhydrite formations) are presented in Figures 26–28) for Model I, Model II, and Model III, respectively. This analysis can be summarized as follows:

- gas migration through the main dolomite formations of the sequestration zone is much faster than its subsequent migration through the Lower Anhydrite, Old Rock Salt, Upper Anhydrite formations of the overburden due to a very low permeability of the latter—as a consequence the gas migration in this part of the overburden is confined to the vertical, upward movement within the fracture with no horizontal spread,
- when the gas reaches the Main Dolomite formation of low thickness and increased permeability it migrates horizontally within this formation,
- as a consequence of this horizontal migration, further gas upward migration is horizontally spread even though it takes place in low permeability formations (Basic Anhydrite, Gray Rock Salt Clay, Major Anhydrite, Young Rock Salt, Red Rock Salt Clay, Transitional Claystone, Young Rock Salt),
- in general, patterns of gas migration in the overburden of the analyzed case are independent of the fracture properties (Model I and Model II for infinite and finite conductivity fracture, respectively)—Figures 25 and 26,
- a distinct, quantitative difference occurs between the cases of different boundary conditions (Model I and Model II of a constant pressure at the overburden bottom vs. Model III of naturally decreasing pressure at that boundary)—Figures 25 and 26 vs. Figure 27. However, the overall pattern of the gas migration in Model III is similar to the pattern of the former models,
- the infinite conductivity fracture is completely filled with gas during the total simulation period and along the complete fracture length and reveals no pressure gradient,
- in contrary, the case of the finite conductivity fracture results in gas saturation varying with the fracture height and changing its value between 15% at the dolomite formations and 1.5% at the anhydrite formations. This indicates a noticeable inflow of formation water into the fracture.

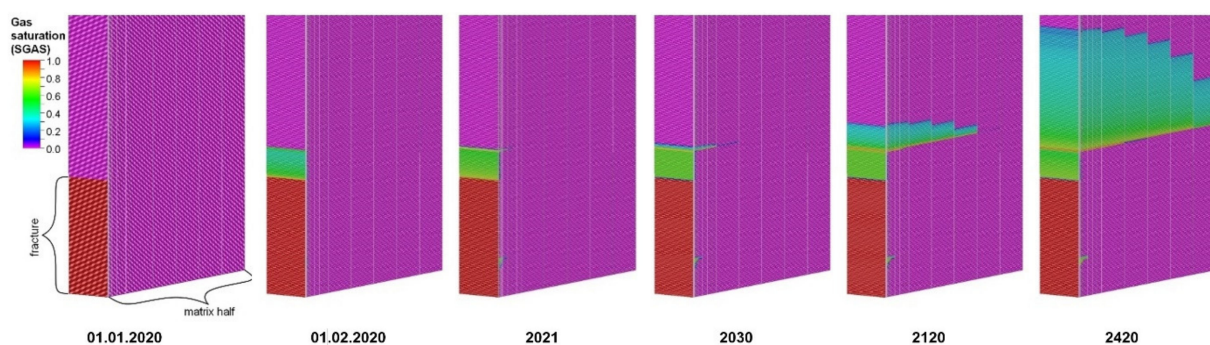


Figure 26. CO₂ migration in the fracture and pores of the overburden rocks. Distribution of CO₂ saturation as a function of time. Model I, Sub-scenario 3.

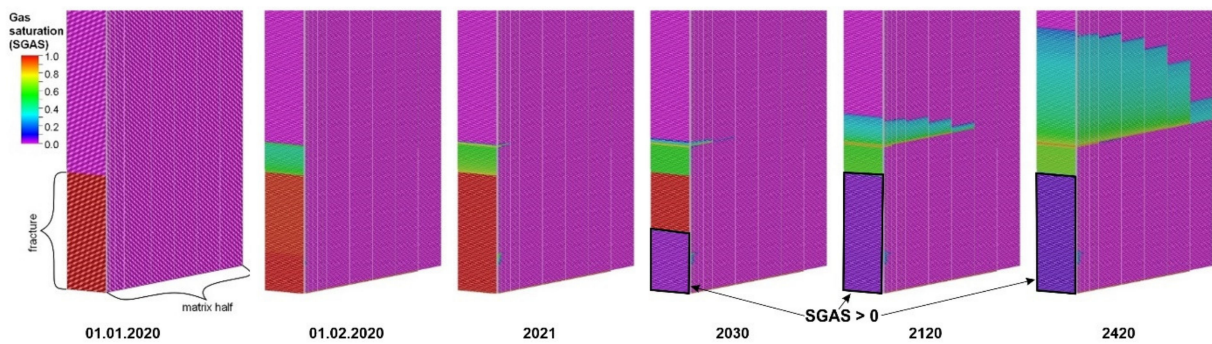


Figure 27. CO₂ migration in the fracture and pores of the overburden rocks. Distribution of CO₂ saturation as a function of time. Model II, Sub-scenario 3.

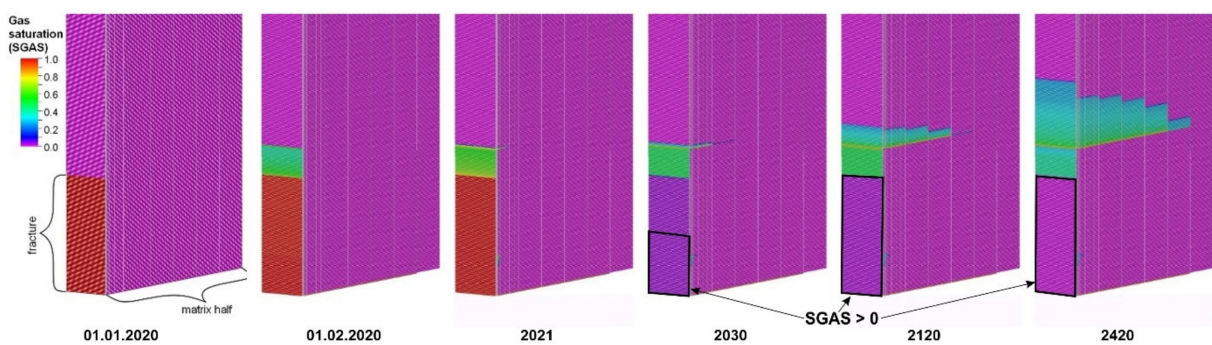


Figure 28. CO₂ migration in the fracture and pores of the overburden rocks. Distribution of CO₂ saturation as a function of time. Model III, Sub-scenario 3.

9. Summary

Numerical simulations of dynamical phenomena taking place during the project of CO₂ sequestration in a partially depleted reservoir gas give a unique opportunity to study reservoir fluid migrations in both the sequestration zone and in the overburden of that zone in case of CO₂ leakage from the sequestration zone to the overburden. Key types of reservoir fluid migrations include: viscous multiphase transport (mobile injected CO₂ in free phase or hypocritical phase, mobile formation water with dissolved CO₂) in porous and naturally fractured media driven by the pressure potential gradient; convection transport due to differences of local fluid densities (downward movement of formation water with dissolved CO₂). The viscous transport is limited by the adhesive phenomena generating immobile phases as a fracture of the free or hypocritical phases. In addition, the injected CO₂ migration is affected by chemical reactions of aquas CO₂ with metal cations. All the above effects, that determine actual migrations of reservoir fluids including the injected CO₂, are modelled in the numerical simulation approach to analyse the process of CO₂ sequestration in partially depleted petroleum reservoirs.

A sequestration capacity being a fundamental characteristic property of the sequestration structure results from a maximum injection volume for which reservoir fluid migrations are constrained to the sequestration zone or, equivalently, no leakage effects occur. Reservoir fluid migrations can generate one of the following, commonly identified four types of leakage risks associated with leakage pathways:

- leakage beyond the structural trap,
- leakage to the caprock by exceeding caprock threshold pressure,
- leakage along activated fractures or other rock discontinuities,
- leakage along well trajectories (deterioration of well integrity).

In this study the numerical approach with all its advantages was applied to realistic structure of a partially depleted gas reservoir located in the southern part of the Pre-

Sudetic Monocline of Poland. A model of this structure was constructed and calibrated against the multi-year history of gas production from the reservoir and acid gas sequestration to the underlying water formations. The sequestration capacity of the structure was determined taking account all the leakage risks by including the above-described migration phenomena and accepting several technical constraints (system of injection wells, their location and completion, maximum allowable injection rates, maximum bottomhole injection pressure). In addition, the following structure characteristics are found significant for the sequestration process simulations: spill points of the analysed structure trap, formation damage (fracturing) pressure, displacement threshold pressure across the reservoir-caprock boundary. The leakage risk associated with deteriorations of injection well integrities was not considered in the above studies as it is an individual feature of injection wells and it cannot be predicted in a deterministic way.

When the sequestration capacity of the structure is exceeded by the injected volume then one or more of the above leakage pathways become effective in the following sequence with the increasing injection volume: beyond the structural trap, to the caprock by exceeding threshold pressure, along activated fracture. For the detailed studies of the migration processes leading to the above leakages, they were investigated separately, one at a time.

In the case of the leakage beyond the structural trap, it is found to extend to the future far beyond the end of an injection phase, i.e., the leakage is observed during the long-time (above 100 years) of a relaxation phase. The total leakage volume strongly depends upon the difference between the sequestration capacity and the actual injection volume. In case of the analysed structure, exceeding the sequestration capacity by 105% results in the total leakage of 1.25% of the sequestration capacity after 100 years of the sequestration project. The analysis of the simulation results also provides an information about the leaked CO₂ spatial distribution beyond the structural trap.

In the case of the leakage to the overburden caused by the pressure step across the sequestration zone-caprock boundary to exceed displacement threshold pressure, in general, depends upon the injected volume (maximum pressure at the sequestration zone top) and transport properties of the overburden formations. While the effect of the total injected volume upon the leakage volume is obvious, then the leaked gas migration in the overburden is significantly dependent upon the detailed properties of individual overburden formations. As the properties of overburden formations are known with typically large uncertainties, such are the simulation results of the total leakage volume. In the case of the analysed structure, the most influential, fundamental properties (absolute permeability, maximum gas relative permeability, critical gas and water saturation, threshold pressure) of the overburden formations were identified and assumed to be known with uncertainties of approx. 30% and to follow triangular or log-triangular distribution functions. The simulation results for the total CO₂ leakage (after 500 years of the sequestration project) to the overburden followed the probability distribution of the normal type with the expected values from 2.7 ‰ to 3.9 ‰ (for the pressure step at the sequestration zone-caprock boundary exceeding the threshold pressure by 12 bars and 17 bars, respectively) of the sequestration capacity and with the standard deviation of 0.6 ‰ of the sequestration capacity. The analogous simulation results for the migration distance of the CO₂ to the overburden followed a probability distribution resembling the normal distribution but with a positive skewness and with the expected values from 4.75 m to 5.75 m with the standard deviation of approximate 1 m.

In the case of the leakage to the overburden caused by a macro-fracture induced by the actual pore pressure exceeding formation damage pressure the CO₂ migration in the overburden depends upon the initial pressure in the sequestration zone, extension, and transport properties of the macro-fracture in the overburden and transport properties of the overburden formations. While the independence upon the first two factors is obvious, the effects of the macro-fracture and overburden properties are strongly dependent upon the relative relations of the properties and the sequence of the formations. In the case of

the analysed structure, the CO₂ migration in the overburden is basically limited to the 2D plane of the fracture interior. This rule results from a typical large disproportion of fracture permeability and matrix permeability in the overburden. If this disproportion is smaller than the CO₂ migration can accept a 3D character as it is the case of the analysed structure at the dolomite, large permeability formation to be followed by the anhydrite, low permeability formation. Unexpectedly, in this case, the migration processes weakly depend upon the transmissibility of the macro-fracture.

10. Conclusions

The studies presented in this paper and concerning the analysis of reservoir fluid migration in the process of CO₂ sequestration in a partially depleted gas reservoir prove usefulness and necessity of the sequestration project modelling in the quantitative characterization of the project. As shown for the analysed case, a detailed description of the reservoir fluid migration corresponding to the injected gas leakage beyond the sequestration zone are strongly dependent upon the details of the geological properties of the structure and cannot be easily deduced from the overall description of the structure. This conclusion implies necessity of the usage of reliable simulation models of the sequestration site and its surrounding. Such models can be constructed only based upon the detailed characterization of the sequestration structure and the complete set of the historical data of the structure functioning including monitoring measurements of the sequestration process and thus improve their reliability and validity.

In particular, this conclusion concerns a long-term leakage risk analysis due to prolonged processes of the leaked gas migration from the sequestration zone to the structural overburden. Only the long-term simulation modelling of a sequestration project is a unique source of information necessary to assess consequences of the leakage.

Author Contributions: Conceptualization, W.S.; methodology, W.S. and K.M.; software, K.M.; validation, W.S.; formal analysis, W.S.; investigation, W.S. and K.M.; resources, W.S. and K.M.; data curation, W.S. and K.M.; writing—original draft preparation, W.S.; writing—review and editing, W.S.; visualization, W.S. and K.M.; supervision, W.S.; project administration, W.S. All authors have read and agreed to the published version of the manuscript.

Funding: The article is based on the statutory work entitled “Poszerzona analiza migracji płynów złożowych w procesie powrotnego zatłaczania gazów kwaśnych do złoża” (in Polish), translated title “Extended analysis of the migration of reservoir fluids in the process of acid gas reinjection into a reservoir”—the work of the Oil and Gas Institute—National Research Institute commissioned by the Ministry of Science and Higher Education; case archive number: DK-4100-3/20, internal order number INIG—PIB: 15/KZ.

Institutional Review Board Statement: Not applicable.

Informed Consent Statement: Not applicable.

Data Availability Statement: The data that support the findings of this study are available on reasonable request from the corresponding author.

Conflicts of Interest: The authors declare no conflict of interest.

References

1. Lubaś, J.; Szott, W. 15-year experience of acid gas storage in the natural gas structure of Borzęcin—Poland. *Nafta-Gaz* **2010**, *66*, 333–338.
2. Lubaś, J.; Szott, W.; Jakubowicz, P. Effects of Acid Gas Reinjection on CO₂ Concentration in Natural Gas Produced from Borzęcin Reservoir. *Nafta-Gaz* **2012**, *68*, 405–410.
3. Lubaś, J.; Stopa, J. Re-injection of toxic gases into water saturated zones of gas reservoirs. *Górnictwo* **1997**, *21*, 23–39.
4. Polish Oil and Gas Company. Historical Production Data of the Borzęcin Reservoir—Reportet by Polish Oil and Gas Company (POGC)—Various Reports in Free Format 1972–2019. Unpublished work, 2019.
5. Mathieson, A.; Midgely, J.; Wright, I.; Saoula, N.; Ringrose, P. In Salah CO₂ Storage JIP: CO₂ sequestration monitoring and verification technologies applied at Krechba, Algeria. *Energy Procedia* **2011**, *4*, 3596–3603. [[CrossRef](#)]

6. Eiken, O. *Twenty Years of Monitoring CO₂ Injection at Sleipner*; Cambridge University Press: Cambridge, UK, 2019; pp. 209–234. [[CrossRef](#)]
7. Qi, L.; Guizhen, L. Risk Assessment of the Geological Storage of CO₂: A Review. In *Geologic Carbon Sequestration*; Springer: Cham, Switzerland, 2016; Chapter 13, pp. 249–284. Available online: <https://www.springerprofessional.de/en/risk-assessment-of-the-geological-storage-of-co2-a-review/10098344> (accessed on 1 July 2021).
8. Sorai, M.; Fujii, T.; Kano, Y.; Uehara, S. Experimental Study on Seal Integrity: The Correlation Between Threshold Pressure and Permeability in a Supercritical CO₂-Water System. *Energy Procedia* **2014**, *63*, 5602–5606. [[CrossRef](#)]
9. Roberts, J.; Wilkinson, M.; Naylor, M.; Shipton, K.; Wood, A.; Haszeldine, S. *Natural CO₂ Sites in Italy Show the Importance of Overburden Geopressure, Fractures and Faults for CO₂ Storage Performance and Risk Management*; Special Publications; Geological Society: London, UK, 2017; Volume 458, pp. 181–211. [[CrossRef](#)]
10. Alexander, D.; Boodlal, D. Evaluating the effects of CO₂ Injection in Faulted Saline Aquifers. *Energy Procedia* **2014**, *63*, 3012–3021. [[CrossRef](#)]
11. Yang, S.; Li, Y.; Zhu, Y.; Liu, D. Effect of fracture on gas migration, leakage and CO₂ enhanced shale gas recovery in Ordos Basin. *Energy Procedia* **2018**, *154*, 139–144. [[CrossRef](#)]
12. Nakajima, T.; Xue, Z.; Chiyonobu, S.; Azuma, H. Numerical Simulation of CO₂ Leakage along Fault System for the Assessment of Environmental Impacts at CCS Site. *Energy Procedia* **2014**, *63*, 3234–3241. [[CrossRef](#)]
13. Brydie, J.; Perkins, E.; Fisher, D.; Girard, M.; Valencia, M.; Olson, M.; Rattray, T. The Development of a Leak Remediation Technology for Potential Non-Wellbore Related Leaks from CO₂ Storage Sites. *Energy Procedia* **2014**, *63*, 4601–4611. [[CrossRef](#)]
14. Doherty, B.; Vasylykivska, V.; Huerta, N.J.; Dilmore, R. Estimating the Leakage along Wells during Geologic CO₂ Storage: Application of the Well Leakage Assessment Tool to a Hypothetical Storage Scenario in Natrona County, Wyoming. *Energy Procedia* **2017**, *114*, 5151–5172. [[CrossRef](#)]
15. Zhang, G.; Lu, P.; Ji, X.; Zhu, C. CO₂ Plume Migration and Fate at Sleipner, Norway: Calibration of Numerical Models, Uncertainty Analysis, and Reactive Transport Modelling of CO₂ Trapping to 10,000 Years. *Energy Procedia* **2017**, *114*, 2880–2895. [[CrossRef](#)]
16. Zapata, Y.; Kirstensen, M.R.; Huerta, N.; Brown, C.; Kabir, C.S.; Reza, Z. CO₂ geological storage: Critical insights on plume dynamics and storage efficiency during long-term injection and post-injection periods. *J. Nat. Gas Sci. Eng.* **2020**, *83*, 103542. [[CrossRef](#)]
17. Diao, Y.; Zhu, G.; Li, X.; Bai, B.; Li, J.; Wang, Y.; Zhao, X.; Zhang, B. Characterizing CO₂ plume migration in multi-layer reservoirs with strong heterogeneity and low permeability using time-lapse 2D VSP technology and numerical simulation. *Int. J. Greenh. Gas Control* **2020**, *92*, 102880. [[CrossRef](#)]
18. Mackay, E.J. 3—Modelling the injectivity, migration and trapping of CO₂ in carbon capture and storage (CCS). In *Geological Storage of Carbon Dioxide (CO₂)*; Woodhead Publishing: Sawston, UK, 2013; pp. 45–67, 68e–70e. [[CrossRef](#)]
19. Khan, C.; Amin, R.; Madden, G. Effects of CO₂ and acid gas injection on enhanced gas recovery and storage. *J. Pet. Explor. Prod. Technol.* **2013**, *3*, 55–60. [[CrossRef](#)]
20. Szott, W.; Gołabek, A.; Miłek, K. Simulation studies of acid gas sequestration in aquifers underlying gas reservoirs. *Prace Inst. Nafty Gazu* **2009**, *165*, 1–89.
21. Szott, W.; Łętkowski, P.; Gołabek, A.; Miłek, K. Modelling of the Long-Term Acid Gas Sequestration and Its Prediction: A Unique Case Study. *Energies* **2020**, *13*, 4701. [[CrossRef](#)]
22. Lubaś, J.; Szott, W.; Łętkowski, P.; Gołabek, A.; Miłek, K.; Warnecki, M.; Wojnicki, M.; Kuśnierczyk, J.; Szuflińska, S.; Biały, S. Long-term sequestration process in the Borzęcin structure—Observation evidence of the injected acid gas migration and possible leakage. *Prace Naukowe Inst. Nafty Gazu* **2020**, *230*, 176.
23. Guo, B.; Lyons, W.C.; Ghalambor, A. *Petroleum Production Engineering, A Computer-Assisted Approach*; Elsevier Inc.: Amsterdam, The Netherlands, 2007. [[CrossRef](#)]
24. Słota-Valim, M.; Gołabek, A.; Szott, W.; Sowizdział, K. Analysis of Caprock Tightness for CO₂ Enhanced Oil Recovery and Sequestration: Case Study of a Depleted Oil and Gas Reservoir in Dolomite, Poland. *Energies* **2021**, *14*, 3065. [[CrossRef](#)]
25. Tahmasebi, P. Multiple Point Statistics: A Review. In *Handbook of Mathematical Geosciences*; Springer: Cham, Switzerland, 2018; pp. 613–643. [[CrossRef](#)]
26. Tahmasebi, P.; Kamrava, S. A pore-scale mathematical modeling of fluid-particle interactions: Thermo-hydro-mechanical coupling. *Int. J. Greenh. Gas Control* **2019**, *83*, 245–255. [[CrossRef](#)]
27. Zhang, X.; Tahmasebi, P. Effects of Grain Size on Deformation in Porous Media. *Transp. Porous Media* **2019**, *129*, 321–341. [[CrossRef](#)]
28. Warnecki, M.; Wojnicki, M. Monitoring of Acid Gas Migration in the Borzęcin Structure. Unpublished work, 2021.